Electronic Supplementary Material (ESI) for Physical Chemistry Chemical Physics
This journal is © The Owner Societies 2011

Electronic Supplementary Information for:

Definitive Solid-State $^{185/187}$Re NMR Spectral Evidence for and Analysis of the Origin of High-Order Quadrupole-Induced Effects for I = 5/2

Cory M. Widdifield,[a] Alex D. Bain,[b] and David L. Bryce[a]*

*Author to whom correspondence is to be addressed. E-mail: dbryce@uottawa.ca

[a] Department of Chemistry and Centre for Catalysis Research and Innovation, University of Ottawa, 10 Marie Curie Pvt., Ottawa, Ontario, Canada.

Tel.: +1 613 562 5800 ext. 2018; Fax: +1 613 562 5170.

[b] Department of Chemistry and Chemical Biology, McMaster University, 1280 Main St. W., Hamilton, Ontario, Canada.

Electronic Supplementary Material (ESI) for Physical Chemistry Chemical Physics
This journal is © The Owner Societies 2011

Table of Contents

Electronic Supplementary Material (ESI) for Physical Chemistry Chemical Physics
This journal is © The Owner Societies 2011

Additional Experimental.

Confirmation of sample purity. In addition to the $^{185/187}$Re NQR experiments presented here, sample purity was confirmed by the manufacturer based upon gravimetric analysis (using tetraphenylarsonium chloride), powder X-ray diffraction (pXRD, NH_4ReO_4 only), and inductively coupled plasma mass spectrometry (ICP-MS). Detailed results of the pXRD and ICP-MS experiments may be obtained by visiting www.sigmaaldrich.com and noting the appropriate lot numbers: NH_4ReO_4 (MKBB7440); $NaReO_4$ (17920CH).

Choice of Hahn or Solomon echo pulse sequence. Relative to the Hahn echo sequence, the Solomon echo sequence allows for a more uniform excitation of a static SSNMR spectrum for a half-integer quadrupolar nucleus.[1] This comes at the expense of signal intensity, where the Hahn echo sequence is superior by a factor of 2. At 21.1 T, sufficient $^{185/187}$Re signals were often available (i.e., experiment times for the collection of each sub-spectrum were around 15 minutes), and thus the Solomon echo was used. At 11.75 T, it was determined that the increased signal would be preferred, leading to the choice of the Hahn echo sequence.

Details pertaining to the generation of Figure 5. In order to generate Figure 5, additional line shape effects, such as chemical shift anisotropy (CSA), dipole-dipole, *J*, etc., were not included and we consider only the case when $I = 5/2$ and $\eta_Q = 0$. Under these assumptions, a model which exactly includes the quadrupole interaction (QI) will give the correct results for the parameters δ_{iso} and C_Q, while second-order perturbation theory will produce values that are somewhat in error. It is noted that only the relative value between the Larmor frequency (ν_0) and the quadrupole frequency (ν_Q) are important. Only the central-transition (CT) frequencies are considered. For an axial electric field gradient (EFG), the high-frequency CT discontinuity corresponds to a crystallite orientation such that V_{33} is perpendicular to B_0 and the low-frequency CT discontinuity corresponds to a crystallite orientation such that V_{33} makes an angle of ca. 41.81° (i.e., the solution to $\cos(\theta) = 5^{1/2}/3$) with respect to B_0.[2] The central (i.e., "step") discontinuity corresponds to a crystallite where V_{33} is parallel to B_0 and hence is unaffected by the QI. Under the current conditions, one needs only to calculate the transition frequencies at these three "critical" points. These critical point CT frequencies may be calculated under second-order perturbation theory for $I = 5/2$ and $\eta_Q = 0$:[3]

$$\nu_{CT,high} = \nu_0 + \frac{\nu_Q^2}{2\nu_0}, \quad \textbf{(1)}$$

$$\nu_{CT,low} = \nu_0 - (8/9)\frac{\nu_Q^2}{\nu_0}, \quad \textbf{(2)}$$

where **(1)** specifies the position of the high-frequency discontinuity ($\nu_{CT,high}$) and **(2)** specifies the position of the low-frequency discontinuity ($\nu_{CT,low}$). Recall that the central discontinuity position is unaffected by the QI.

For the exact simulations, while it is true that the high-frequency discontinuity corresponds to the case where V_{33} is perpendicular to B_0 and that the central discontinuity corresponds to the crystallite where V_{33} is parallel to B_0, the crystallite orientation corresponding to the low-frequency discontinuity will vary as a function of ν_0/ν_Q. For large ν_0/ν_Q values (i.e., strong Zeeman interaction), it is such that the angle roughly corresponds to 41.81°, but as the ν_0/ν_Q value decreases, the V_{33}/B_0 angle will change such that its value will be reduced. A plot of this dependence is shown in Figure S4. In any event, for the exact QI simulations, three critical points exist. The CT frequencies were calculated at these critical orientations under both the exact and second-order perturbation theory models assuming a variety of ν_0/ν_Q values, the results of which are tabulated in Table S3 and depicted in Figure 5. Once the transition frequencies at the critical points are known, the C_Q and δ_{iso} values can be determined from second-order perturbation theory line shape models in a relatively straightforward fashion: ν_Q is related to the span in frequency between the high- and low-discontinuities ($\Delta\nu$) for the CT using the following equation (i.e., by taking the difference between **(1)** and **(2)**):

$$\Delta\nu = \nu_{CT,high} - \nu_{CT,low} = (25/18)\frac{\nu_Q^2}{\nu_0}. \qquad \textbf{(3)}$$

After which C_Q can be determined, as $C_Q = 20\nu_Q/3$ under the conditions considered here.

In general it is observed that for a given C_Q value, second-order perturbation theory will give a line shape width that exceeds the correct value. Hence, to fit the data using second-order perturbation theory would require the apparent C_Q value to underestimate the true value. The amount by which an apparent C_Q value deviated from the true C_Q value (i.e., from exact QI theory) was used to calculate the percentage errors. After scaling to the appropriate line width, the line shape generated using second-order perturbation theory will still be shifted in the positive frequency direction. The correction required to match the CT frequencies for the high- and low-frequency discontinuities is related to the error in the extracted δ_{iso} value. To determine the apparent δ_{iso} value using second-order perturbation theory, a simple frequency shift is applied (always in the negative direction). Hence, the chemical shift arrived at using second-order perturbation theory will always be negative relative to the true value. After these two corrections are implemented, the second-order perturbation theory and exact theory simulations will have high- and low-frequency discontinuities that match. As a result of this procedure, it must be noted that the

Electronic Supplementary Material (ESI) for Physical Chemistry Chemical Physics
This journal is © The Owner Societies 2011

central step discontinuity will not match between the second-order and exact theory models. Indeed, there exists no meaningful case where all three discontinuities would exactly match between the second-order perturbation theory and exact theory simulations.

Electronic Supplementary Material (ESI) for Physical Chemistry Chemical Physics
This journal is © The Owner Societies 2011

Table S1. Detailed $^{185/187}$Re NQR/SSNMR experimental acquisition parameters[a]

$\mathbf{B}_0$ / T	nuclide	window / kHz[b]	points[c]	$\pi/2$ / μs[d]	scans	recycle delay / s	τ_1;τ_2 / μs	details
NH_4ReO_4								
~ 0	^{185}Re	1000	512	1.6	4096	0.1	12.6;10.0	Hahn echo; 4 mm HX MAS probe; $m_I = \pm 3/2 \leftrightarrow \pm 5/2$ transition
~ 0	^{187}Re	1000	512	1.6	4096	0.1	12.6;10.0	Hahn echo; 4 mm HX MAS probe; $m_I = \pm 3/2 \leftrightarrow \pm 5/2$ transition
11.75	$^{185/187}$Re	2000	1024	1.2	17500	0.1	13.2;5.0	VOCS Hahn echo; 31 pieces; offset = 200 kHz; 4 mm HXY MAS probe
21.1	$^{185/187}$Re	2000	1024	1.2	8192	0.1	13.8;9.4	VOCS Solomon Echo; 20 pieces; offset = 300 kHz; 4 mm HX MAS probe
$NaReO_4$								
~ 0	^{185}Re	1000	512	1.1	256	0.1	13.35;4.5	Hahn echo; 4 mm HX MAS probe; $m_I = \pm 1/2 \leftrightarrow \pm 3/2$ transition
~ 0	^{185}Re	1000	512	1.1	256	0.1	13.35;4.5	Hahn echo; 4 mm HX MAS probe; $m_I = \pm 3/2 \leftrightarrow \pm 5/2$ transition
~ 0	^{187}Re	1000	512	1.5	256	0.1	12.75;4.5	Hahn echo; 4 mm HX MAS probe; $m_I = \pm 1/2 \leftrightarrow \pm 3/2$ transition
~ 0	^{187}Re	1000	512	1.1	256	0.1	13.35;5.0	Hahn echo; 4 mm HX MAS probe; $m_I = \pm 3/2 \leftrightarrow \pm 5/2$ transition
11.75	$^{185/187}$Re	2000	512	various, see details	17500	0.09	various, see details	VOCS Hahn echo; 71 pieces; offset = 200 kHz; 4 mm HXY MAS probe; for high frequency (117.687 – 121.287 MHz) subspectra, $\pi/2$ = 1.2 μs and τ_1 = 13.2 μs; for low frequency (93.887 – 104.087 MHz) subspectra, $\pi/2$ = 0.8 μs and τ_1 = 13.8 μs
21.1	$^{185/187}$Re	2000	1024	various, see details	8192	0.09	various, see details	VOCS Solomon echo; 56 pieces; offset = 300 kHz; 4 mm HX MAS probe; for 207.483 – 209.583 MHz subspectra, $\pi/2$ = 1.7 μs and τ_1 = 13.3 μs; for 205.983 – 207.183 MHz subspectra, $\pi/2$ = 1.5 μs and τ_1 = 13.5 μs; for 202.383 – 205.683 MHz subspectra, $\pi/2$ = 1.3 μs and τ_1 = 13.7 μs; for 199.983 – 202.083 MHz subspectra, $\pi/2$ = 1.4 μs and τ_1 = 13.6 μs; for 193.083 – 199.683 MHz subspectra, $\pi/2$ = 1.5 μs and τ_1 = 13.5 μs

[a] Unless denoted otherwise, experiments were conducted at T = 291.8(0.2) K and are under static conditions.
[b] Where applicable, acquisition parameters are for each sub-spectrum.
[c] Complex time-domain data points.
[d] Selective pulses.

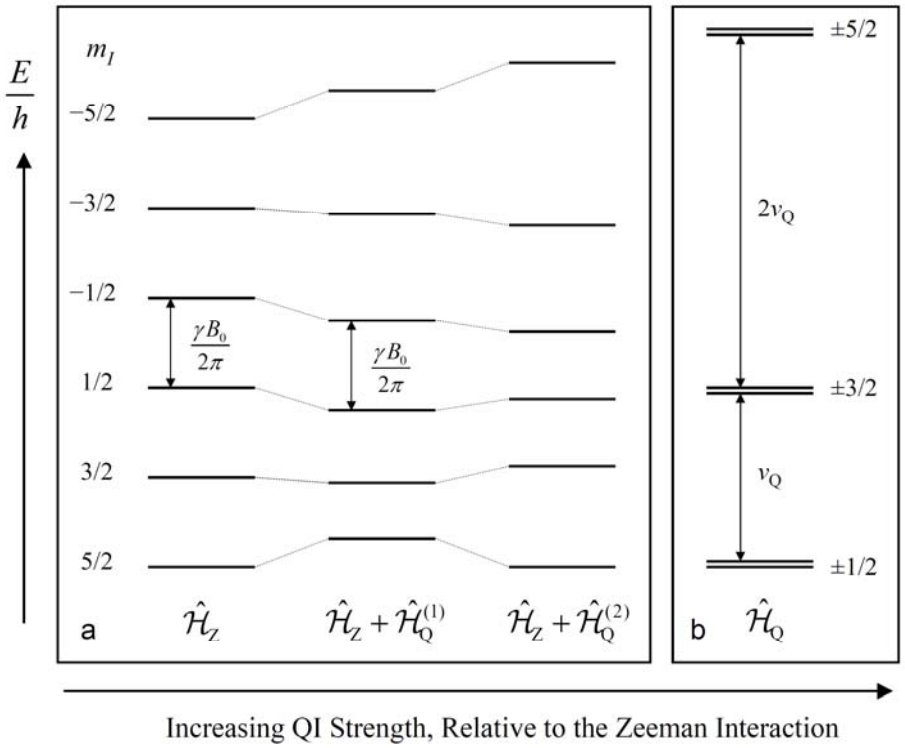

Figure S1. Qualitative energy level diagrams for I = 5/2, which highlight the effects of the QI on the Zeeman eigenstates (i.e., eigenstates under only $\hat{\mathcal{H}}_Z$), as adapted from MacKenzie and Smith.[4] For simplicity, it is assumed that $\eta_Q = 0$. In (a), the relative strength of the QI (as compared to the Zeeman interaction) increases from left to right and the qualitative effects of applying the quadrupolar Hamiltonian using first-order perturbation theory ($\hat{\mathcal{H}}_Q^{(1)}$) and second-order perturbation theory ($\hat{\mathcal{H}}_Q^{(2)}$) on the Zeeman eigenstates is illustrated. As shown in the middle column of (a), the CT frequency is unaffected by the QI to first-order. In (b), the eigenstates are ordered differently than in (a), as the eigenstates are subject to only the QI (i.e., only $\hat{\mathcal{H}}_Q$).

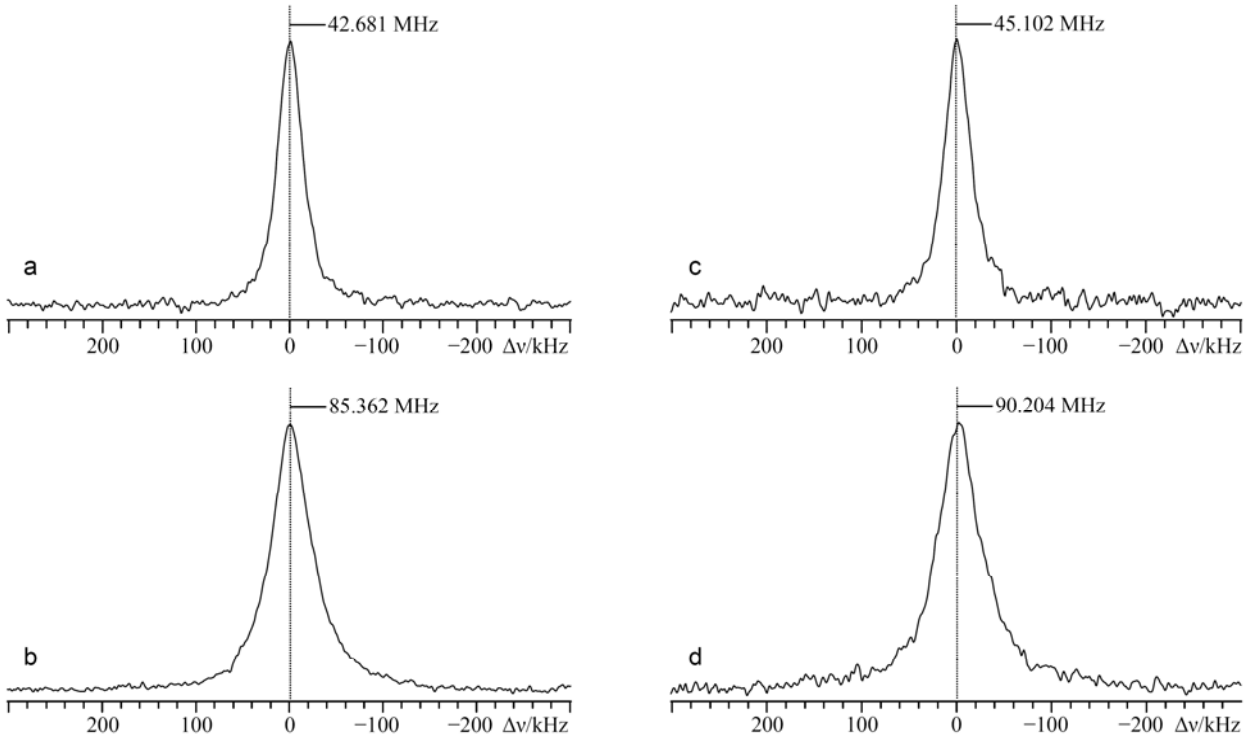

Figure S2. Experimental ^{187}Re (a, b) and ^{185}Re (c, d) NQR spectra of powdered $NaReO_4$, acquired at T = 291.8 K. The transition frequencies are specified in the Figure. (a, c) $m_I = \pm 1/2 \leftrightarrow \pm 3/2$; (b, d) $m_I = \pm 3/2 \leftrightarrow \pm 5/2$, where for all transitions $|\Delta m_I| = 1$.

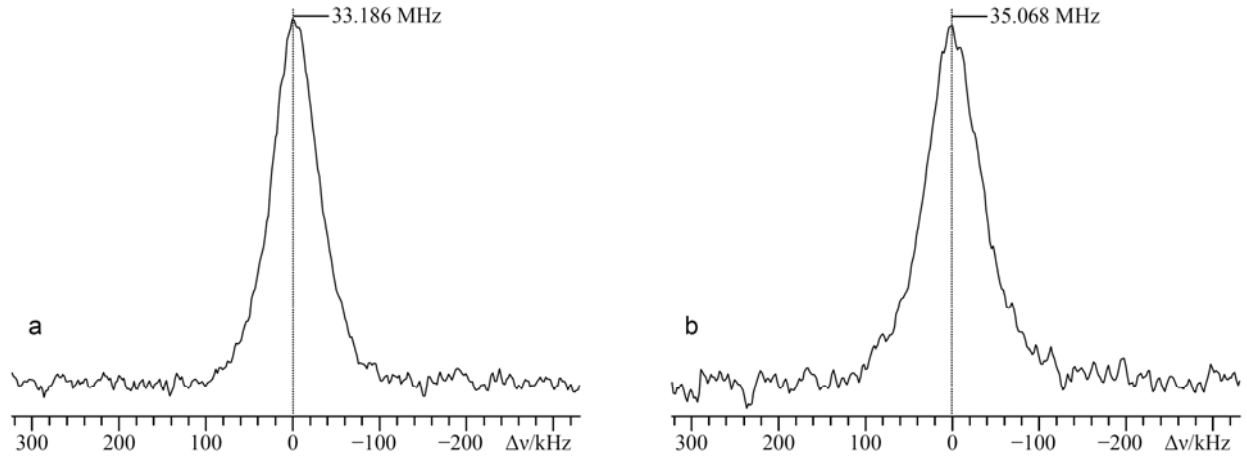

Figure S3. Experimental ^{187}Re (a) and ^{185}Re (b) NQR spectra ($m_I = \pm 3/2 \leftrightarrow \pm 5/2$, where $|\Delta m_I| = 1$) of powdered NH_4ReO_4, acquired at T = 291.8 K. The transition frequencies are specified in the Figure.

Table S2. Experimental $^{185/187}$Re EFG Tensor Parameters and Isotropic Chemical Shifts Obtained via Second-Order Perturbation Theory Modeling of the Quadrupole Interaction[a]

compound	B_0 / T	$\lvert C_Q(^{185}\text{Re})\rvert$[b] / MHz	$\lvert C_Q(^{187}\text{Re})\rvert$ / MHz	η_Q	$\delta_{iso}(^{185}\text{Re})$[c] / ppm	$\delta_{iso}(^{187}\text{Re})$[c] / ppm
$NaReO_4$	21.1	299.8(0.4)	283.9(0.4)	~ 0	−870(50)	−650(50)
NH_4ReO_4	11.75	116.8(0.4)	110.6(0.3)	~ 0	−210(50)	−170(50)

[a] Please note that this table is for comparison purposes (i.e., with Table 1) only. These values are not the correct parameters for the systems under study. They serve to highlight the *errors* associated in using second-order perturbation theory to model the SSNMR line shapes when there is a very large QI. Measurement errors are within parentheses and parameter definitions are as follows: $C_Q = eQV_{33}/h$; $\eta_Q = (V_{11} - V_{22})/V_{33}$, where $|V_{11}| \leq |V_{22}| \leq |V_{33}|$; $\delta_{iso} = (\delta_{11} + \delta_{22} + \delta_{33})/3$, where $\delta_{33} \leq \delta_{22} \leq \delta_{11}$. All measurements were carried out at $T = 291.8(0.2)$ K. SSNMR line shape simulations were performed using WSolids1.[5]
[b] While C_Q may take any real value, $|C_Q|$ is measured experimentally using SSNMR.
[c] Rhenium chemical shifts are relative to 0.1 mol/dm^3 $NaReO_4$ in D_2O ($\delta_{iso}(^{185/187}\text{Re}) = 0$ ppm).

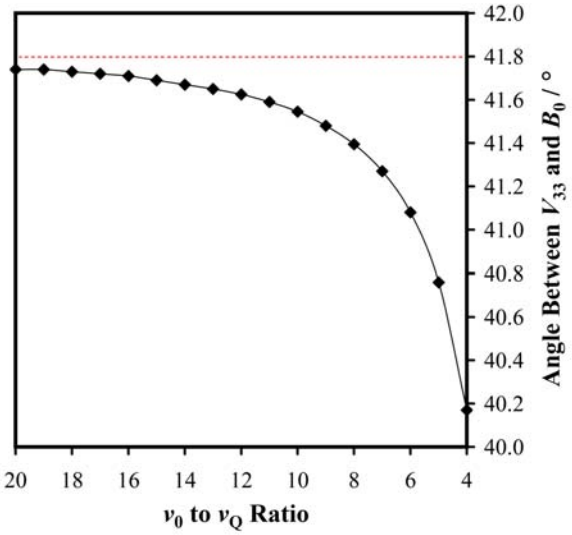

Figure S4. Angle between V_{33} and B_0 corresponding to the low-frequency CT discontinuity as a function of the ν_0 to ν_Q ratio using exact QI simulations. The dashed red line highlights the constant value (i.e., independent of the ν_0 to ν_Q ratio) of 41.81° arrived at using second-order perturbation theory. The points in the graph are connected using a line that is meant to serve as a guide for the eyes only.

Electronic Supplementary Material (ESI) for Physical Chemistry Chemical Physics
This journal is © The Owner Societies 2011

Table S3. Table of Values Used to Construct Figures 5a and 5b[a]

ν_0:ν_Q	C_Q / MHz	ν_Q / MHz	ΔC_Q / MHz[b]	ΔC_Q / %	$\Delta\delta_{iso}$ / kHz[c]	$\Delta\delta_{iso}$ / ppm
20	37.929	5.6894	−0.0095	−0.0250	−0.28444	−2.4998
19	39.927	5.9890	−0.0111	−0.0278	−0.34929	−3.0697
18	42.143	6.3215	−0.0130	−0.0309	−0.43354	−3.8101
17	44.620	6.6934	−0.0155	−0.0347	−0.54480	−4.7879
16	47.413	7.1117	−0.0186	−0.0392	−0.69454	−6.1039
15	50.573	7.5860	−0.0225	−0.0446	−0.89907	−7.9013
14	54.187	8.1280	−0.0277	−0.0512	−1.1849	−10.413
13	58.353	8.7530	−0.0347	−0.0594	−1.5935	−14.004
12	63.213	9.4820	−0.0441	−0.0698	−2.1944	−19.285
11	68.960	10.344	−0.0573	−0.0831	−3.1079	−27.313
10	75.860	11.379	−0.0764	−0.1007	−4.5510	−39.996
9	84.287	12.643	−0.1049	−0.1245	−6.9353	−60.950
8	94.820	14.223	−0.1497	−0.1579	−11.107	−97.610
7	108.367	16.255	−0.2241	−0.2068	−18.946	−166.50
6	126.430	18.964	−0.3576	−0.2828	−35.092	−308.40
5	151.713	22.757	−0.6225	−0.4103	−72.724	−639.13
4	189.647	28.447	−1.2320	−0.6496	−177.36	−1558.7

[a] For these calculations, the ν_0 value was kept constant at 113.787 MHz. Any set of values for ν_0 and ν_Q could have been chosen, as the important quantity is their ratio with respect to one another.
[b] Error in the C_Q value arrived at using second-order perturbation theory. Details are given in the ESI, Additional Experimental.
[c] Error in the δ_{iso} value arrived at using second-order perturbation theory. Details are given in the ESI, Additional Experimental.

References

1 P. R. Bodart, J. P. Amoureux, Y. Dumazy and R. Lefort, *Mol. Phys.,* 2000, **98,** 1545.

2 K. J. Ooms, K. W. Feindel, V. V. Terskikh and R. E. Wasylishen, *Inorg. Chem.,* 2006, **45,** 8492.

3 M. E. Smith and E. R. H. van Eck, *Prog. Nucl. Magn. Reson. Spectrosc.,* 1999, **34,** 159.

4 K. J. D. MacKenzie and M. E. Smith, in *Multinuclear Solid-State NMR of Inorganic Materials*, Pergamon: Amsterdam, 2002, p. 54.

5 K. Eichele and R. E. Wasylishen, *WSolids1: Solid-State NMR Spectrum Simulation Package*, 2009, v. 1.19.11.